A Novel Framework for Parametric Analysis of Coastal Transition Zone Modeling

Taher Chegini (iD), *Gustavo de Almeida Coelho* (iD), *John Ratcliff, Celso M. Ferreira* (iD), *Kyle Mandli* (iD),
Patrick Burke (iD)*, and Hong-Yi Li* (iD)

Research Impact Statement: Introduces a framework for large-scale analyses of physical processes affecting coastal dynamics to assist in planning and management of coastal areas at local to regional scales.

ABSTRACT: Vulnerability of coastal regions to extreme events motivates an operational coupled inland-coastal modeling strategy focusing on the coastal transition zone (CTZ), an area between the coast and upland river. To tackle this challenge, we propose a top-down framework for investigating the contribution of different processes to the hydrodynamics of CTZs with various geometrical shapes, different physical properties, and under several forcing conditions. We further propose a novel method, called tidal vanishing point (TVP), for delineating the extent of CTZs through the upland. We demonstrate the applicability of our framework over the United States East and Gulf coasts. We categorize CTZs in the region into three classes, namely, without estuary (direct river–coast connection), triangular-, and trapezoidal-shaped estuary. The results show that although semidiurnal tidal constituents are dominant in most cases, diurnal tidal constituents become more prevalent in the river segment as the discharge increases. Also, decreasing the bed roughness value promotes more significant changes in the results than increasing it by the same value. Additionally, the estuary promotes tidal energy attenuation and consequently decreases the reach of tidal signals through the upland. The proposed framework is generic and extensible to any coastal region.

(KEYWORDS: rivers/streams; flooding; hydrodynamics; fluvial processes; tides; coastal transition zones.)

INTRODUCTION

Development, operation, and management of infrastructure located in coastal areas require accurate estimations of water level ranges, magnitude, and frequencies in the areas between the coast and the upland where tides no longer influence water level variation, that is, the coastal transition zone (CTZ) (Moritz et al. 2016; Couasnon et al. 2020). For this purpose, an initiative is underway to enhance the

National Water Model (NWM) (NOAA 2016) by including water level predictions in CTZs (Bakhtyar et al. 2020). However, coupling the NWM to existing coastal hydrodynamic models in operational settings presents challenges such as increasing computational complexity and a priori parameter estimations (e.g., Garzon and Ferreira 2016). Understanding the processes that contribute to water levels in CTZs, such as mean sea level, tidal range, river discharge, and storm surge, is essential to tackling these challenges (e.g., Du et al. 2018; Valle-Levinson et al. 2020;

Camus et al. 2021; Ghanbari et al. 2021; Hsiao et al. 2021). The combined effect of these components is called the total water level (TWL) and the contribution of each component may vary based on the location of a CTZ.

Numerous studies mathematically defined the relationships between frictional and topographical factors, and their respective and combined influence on the tidal amplification in estuaries (e.g., Jay 1991; Lanzoni and Seminara 1998; Jena et al. 2018). Some studies have also examined the effects of longitudinally cross-sectional convergence of estuaries on tidal signal propagation. Friedrichs and Aubrey (1994) and Jay (1991) show that convergence significantly influences amplitudes of tidal constituents and velocity fields. Additionally, Lanzoni and Seminara (1998) suggest that the rate of convergence and nonlinear responses, such as the generation of overtides, play a key role in the tidal signal propagation through the upland. Moreover, Talke and Jay (2020) demonstrate the influence and importance of tidal resonance on the amplification of water levels through mathematical analysis.

Many published works feature case studies that examine coastal models' sensitivities to input parameters in specific regions (e.g., Garzon and Ferreira 2016; Sohrt et al. 2021). Akbar et al. (2017) examined the effects of variations in bottom friction on water levels during a landfalling hurricane in the Gulf of Mexico. Moreover, Alebregtse and Swart (2016) use a semi-analytical model to study the effect of river discharge on the propagation of tidal waves in the Yangtze estuary, in China. They show that when increasing river discharge, the amplitude of semidiurnal sea surface elevation decreases. Calero Quesada et al. (2019) study the Guadiana estuary, in Spain and demonstrate that river discharge could influence tidal propagation through estuaries. Harrison et al. (2021) investigate the sensitivity of two UK estuaries to high river discharge and sea-level rise scenarios. Additionally, some other site-specific studies, such as Khalid and Ferreira (2020), Maskell et al. (2014), and Valle-Levinson et al. (2020), demonstrate the significant role of geometric variations in inundation processes, particularly with the interaction between the river and storm surge.

However, Ward et al. (2020) and Harrison et al. (2021) argue that currently, many studies are site specific, and they fall short in advancing our understanding of the dynamic seaward and landward extent of coastal interfaces across the scale. They suggest that researchers should instead steer their concerted effort toward multidisciplinary regional-scale analysis of coastal interfaces. For example, Kerr et al. (2013) present a regional study in the Gulf of Mexico and show that due to energy dissipation at the seafloor, decreasing Manning's roughness results in increases in water levels and vice versa. Joyce et al. (2019) carry out a similar study in Puerto Rico and the United States (U.S.) Virgin Islands and based on the analysis of Hurricanes Irma and Maria conclude that the pressure deficit due to these hurricanes is the main driver in the water level response. Moreover, Du et al. (2018) perform numerical simulations on several idealized domains and nine realistic estuaries over the U.S. East coast, to study the tidal responses to sea-level rise. They demonstrate a reduction in tidal range in narrow channels and large low-lying shallow areas under higher sea levels. Ghanbari et al. (2021) show that the northeast Atlantic and the western part of the Gulf coasts are the most exposed to compound flood hazards based on the assessment of 26 paired tidal-riverine stations on the U.S. coast.

In an effort toward regional-scale analysis of coastal areas, we propose a top-down framework for investigating the contributions of different processes and parameters to TWL prediction in CTZs. This framework takes into account the effects of geometrical shapes, physical properties, and forcing conditions. We achieve this goal in two steps: First, we decompose the complex coastal hydrodynamic system into simpler physical processes according to data analysis of the region of interest. Second, we study these processes individually to gain more insights into their role in coastal dynamics. We carry out such a study on each process through sensitivity analyses of their corresponding model parameters. For this purpose, we perform numerous numerical simulations on idealized domains while relying on a complex coastal model that can capture intricacies of processes that contribute to coastal hydrodynamics. Using idealized domains allows for modeling numerous scenarios and studying the role of contributing processes in isolation. Additionally, this framework provides a novel method called tidal vanishing point (TVP) for delineating the extent of a CTZ through the upland. This extent influences decisions on data exchange locations between an inland and a coastal model (i.e., handoff location), which is an important consideration when optimizing the balance between accuracy and performance. Furthermore, insights into the respective significance of various physical parameters assist coastal modelers in model calibration and achieving computational efficiency by improving estimations of only relevant inputs or features.

This study demonstrates the applicability of the proposed framework by employing it for CTZs across the Gulf of Mexico and the U.S. East Coast, where most of the U.S. coastal areas with socioeconomic importance are located. The structure of the rest of this paper is as follows: First, the Methodology

section describes the details of our proposed framework. Then, the Results and Discussion section present the statistical analyses on the spatially distributed model results for water surface heights and velocity fields, as well as the TVP estimations. The last section provides concluding remarks.

METHODOLOGY

This section describes details of our proposed framework for classifying CTZs and evaluating processes and parameters that influence TWL prediction. Figure 1 depicts a conceptual flowchart of the framework which we categorize into three groups: data analysis, modeling, and assessment.

Data Analysis

The data analysis tasks deal with obtaining ground-truth and remote sensing data from various sources and extracting spatiotemporal summaries that provide insights into hydrodynamic characteristics of the region of interest. We determine these characteristics to parameterize the physical properties and forcing conditions in the region of interest.

Modeling

Upon obtaining summaries of physical properties and forcing conditions in the region of interest, we carry out a series of hydrodynamic simulations on idealized domains with simple geometries. For this purpose, we define a control model (a reference scenario) with some predetermined values for all the model parameters and then systematically perturb the parameters, so we can study their contributions to the changes in the model behavior in isolation.

Assessment

We design the tasks in this category for gaining insights into the relative significance of contributing processes in coastal dynamics. For this purpose, we use the significance test concept for quantifying changes in some variables of interest caused by their perturbations. Additionally, we define a new concept called TVP for characterizing the reach of tidal signals through the upland, that is, the extent of CTZs. The overall goal of the framework is to provide a mathematically rigorous and extensible blueprint for conducting sensitivity analyses on a set of model parameters that characterize the hydrodynamics of CTZs. We note that our proposed framework focuses on the relative significance of the parameters rather than absolute values.

Comparison Metrics (Significance Test). First, we assess the changes between each prediction and the reference scenario for a variable of interest through an error estimation metric such as mean absolute error (MAE) or root-mean-square error to obtain E_1 for the first prediction and E_2 for the second prediction. Then, we compute the mean and standard deviation of the obtained errors. Next, we determine the half-width of the confidence interval at a specified level on the difference between the mean errors ($\Delta E = E_2 - E_1$). We compute this half-width confidence interval using $\text{CI}_\alpha = \sqrt{2(1 - \rho)} \times z^* \frac{\sigma}{\sqrt{n}}$, where ρ is the correlation coefficient (Pearson R) between the scores, σ is the standard deviation, α is the confidence level, z^* is the z-score value corresponding to α (e.g., it is 1.96 for 95% confidence interval), and n is the number of observation points. Finally, we compute $\text{SD} = \text{sign}(\Delta E) \times (abs(\Delta E) - \text{CI}_\alpha)$, which measures the relative significance of the predictions' deviation from the reference scenario. A positive value means that the total change in Scenario 2 is more significant than the total change in Scenario 1 and vice versa for a negative value.

Tidal Vanishing Point. To determine the extent of CTZ's influence through the upland, we devise a procedure based on fluctuations of the tidal constituents' amplitudes across the centerline of the domain. This method relies on the amplitudes of the tidal constituents from the water level time series at grid points along the domain's centerline that extends from the ocean boundary to the river discharge boundary. The computation procedure is as follows:

1. Determine the dominant tidal constituent(s) within each tidal constituent category based on their amplitudes: Semidiurnal, diurnal, short period, and long period.
2. Determine the (signal) filtering window size based on a percentage of the centerline length. This percentage is a parameter that we can determine via trial-and-error.
3. Carry out three subsequent passes of low-pass filtering on the amplitudes.
4. Compute exceedance probability for the filtered amplitudes.
5. Determine a threshold for amplitudes of each constituent, below which we consider the fluctuations negligible. We determine this threshold with trial-and-error based on a percentage of the exceedance probability.
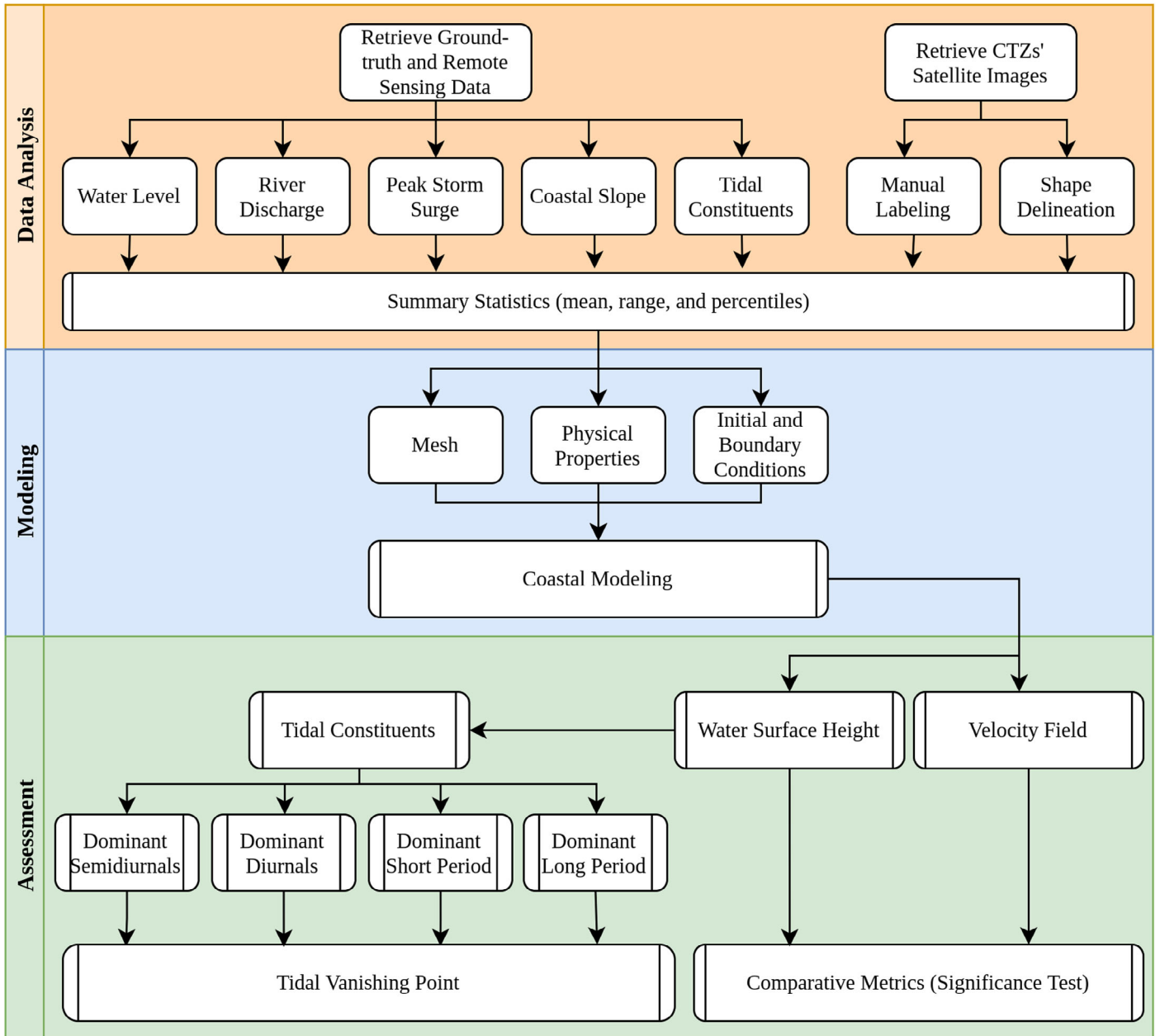
FIGURE 1. Flowchart showing the framework for studying the contribution of parameters affecting total water level prediction. CTZ, coastal transition zone.

6. Compute locations across the centerline where the amplitudes onward fall below the thresholds for each constituent. We coin these locations' TVPs. In some cases, we might not reach a TVP due to not long enough river length.

7. Aggregate the obtained TVPs by finding their maximum value for each constituent.

We elucidate all these steps through their application in a case study in the following section. Moreover, we note that extending the TVP concept from idealized domains to real coastal domains can be challenging due to its reliance on the trial-and-error method and the simplifications. Therefore, since this study applies this method to a subset of coastal areas, the extent of applicability of TVP for determining the reach of CTZs requires further analyses.

CASE STUDY

In this section, we demonstrate the details of our framework through its application across the U.S. East and Gulf coasts.

Data Analysis

Retrieve Ground-Truth and Remote Sensing Data. At the first step, we retrieve the required datasets in our study region (Table 1) and conduct a series of statistical analyses on them to obtain sensible ranges for the parameters that we need to support the model generation and define boundary conditions for simulation scenarios.

According to the obtained water level observations, tides vary significantly over the study region, wherein amplitudes are smaller in the Gulf Coast than the East Coast. We evaluate the water level data from all monitoring stations in the study region under the tidal influence to determine the spatial distribution of the strongest tidal constituents in the region. As shown in Figure 2a, based on data from the period 2000–2015, the M2 (principal lunar semidiurnal) tidal constituent is the strongest over the East and most of Florida coast, while the K1 (a lunar diurnal constituent) is often the strongest tidal constituent in the Gulf. Figure 2b and 2c shows the seasonal variation of the mean range tide (MN) of the two strongest constituents (M2 and K1) where the mean tide range of K1-dominant stations has higher seasonal variability when compared with the M2-dominant stations. The mean tide range is the difference in height between mean high water and mean low water (NOAA 2020). Although there are two types of dominant tides in the region, we only consider an M2-dominant tide in this study.

For determining limits of river discharge in the region, we use HyRiver (Chegini et al. 2021) Python package to collect mean daily discharge data from U.S. Geological Survey (USGS) monitoring stations located in streams where the processes in estuaries influence the flow (Figure 3a). The USGS classifies the interaction between the stream and ocean waters into tide stream (ST-TS) and estuary (ES).

An ST-TS station is located where the streamflow is influenced by the tide, but the water chemistry is not normally influenced. An ES station is located at the coastal inlet of the ocean where the water normally mixes with stream water (USGS 2021). Out of 390 ST-TS and ES stations, 26 have mean daily discharge data that we use for computing a summary of discharges in our study region (Figure 3b). We consider the mean of means (Equation 1) as the lower limit and the mean of peaks (Equation 2) as the upper limit for the river discharge values at the upstream boundary. We compute these two mean values using:

$$\mu_{\bar{x}} = \frac{\sum \bar{x}_i}{n}, \quad (1)$$

$$\mu_y = \frac{\sum y_i}{n}, \quad (2)$$

where $\mu_{\bar{x}}$ is the mean of means, $\bar{x}_i$ is the mean discharge for station i, μ_y is the mean of peaks, y_i is the peak discharge for station i, and n is the total number of stations.

At the next step, we determine the range of peak storm surge heights based on a statistical analysis of extreme water level data over the study region and in the period 2000–2015. The extreme water levels (Figure 4a) are 1% exceedance probability of water levels above mean higher high water (MHHW). MHHW is the tidal elevation determined by averaging the higher of each day's two high tides at a particular location over a recorded history (NOAA 2020). We consider the minimum (0.769 m) and the maximum (3.154 m) values of the data as the lower and higher limits for the peak storm surge height, respectively.

The bed slope is another important physical property that influences coastal dynamics. We obtain the limits of this parameter in the Gulf and East coasts from Hammar-Klose and Thieler (2001). Figure 4b presents the coastal slope map of the region, where the slope varies from 0 in the Gulf region to over 0.4% in the upper regions of the East coast.

Classification of CTZs. We define a series of idealized domains based on a classification of river-estuary systems (RESs) in the study region. For this purpose, we retrieve over 400 black and white satellite images of the RESs from the Stamen (2019, http://maps.stamen.com/) map service. We opt for black and white images to facilitate their visual inspection in the next step, that is manual labeling. We sift through the images and delineate the smallest enclosing polygon for each RES (Figure 5a–5c).

TABLE 1. Datasets for obtaining sensible ranges for model parameters.

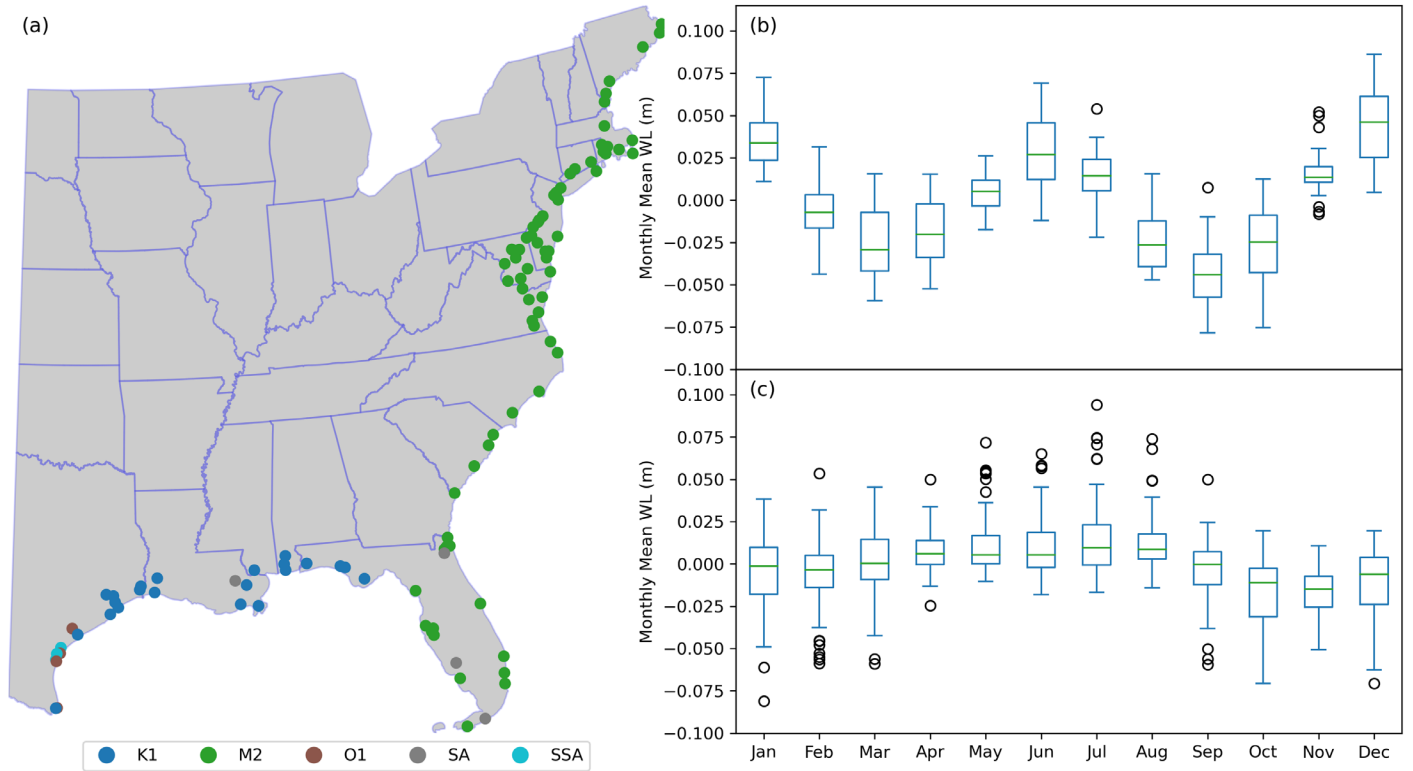| Dataset	Source	Period
Water level observations	Oceanographic Products and Services (CO-OPS)	2000–2015
Extreme water levels	CO-OPS	2000–2015
Mean daily river discharge	National Water Information System (NWIS)	2000–2015
Coastal slope	Hammar-Klose and Thieler (2001)	—
Tidal constituents	CO-OPS	—
Satellite images	Stamen (2019, http://maps.stamen.com/) and Google Earth Pro	—

FIGURE 2. (a) Map showing the strongest tidal constituents at National Oceanic and Atmospheric Administration (NOAA) water level stations, and monthly mean water level (WL) variations (datum is mean sea level) for (b) K1 ($n = 19$) and (c) M2 ($n = 66$) dominant stations.
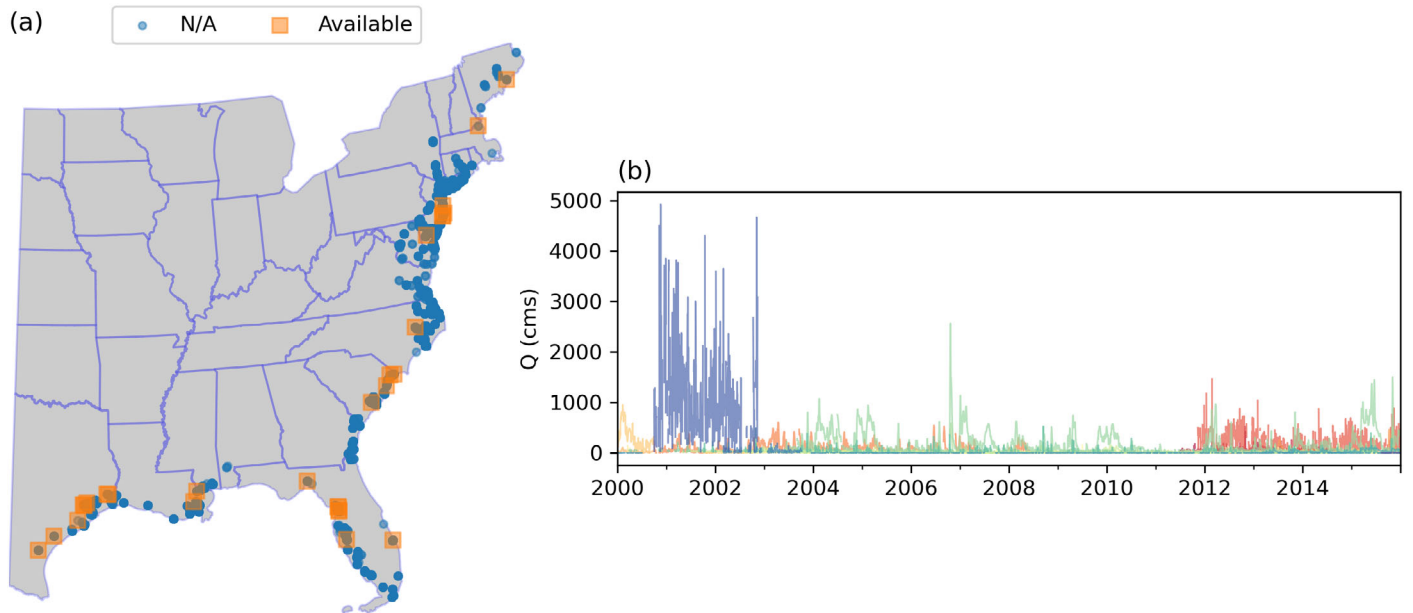

FIGURE 3. (a) Map showing the location of United States Geological Survey stations under the tidal influence with ($n = 29$) and without ($n = 361$) available mean daily discharge data after 2000; (b) discharge data at the selected 29 stations for the period 2000–2015 (mean of means = 90 m^3/s and mean of peaks = 570 m^3/s).
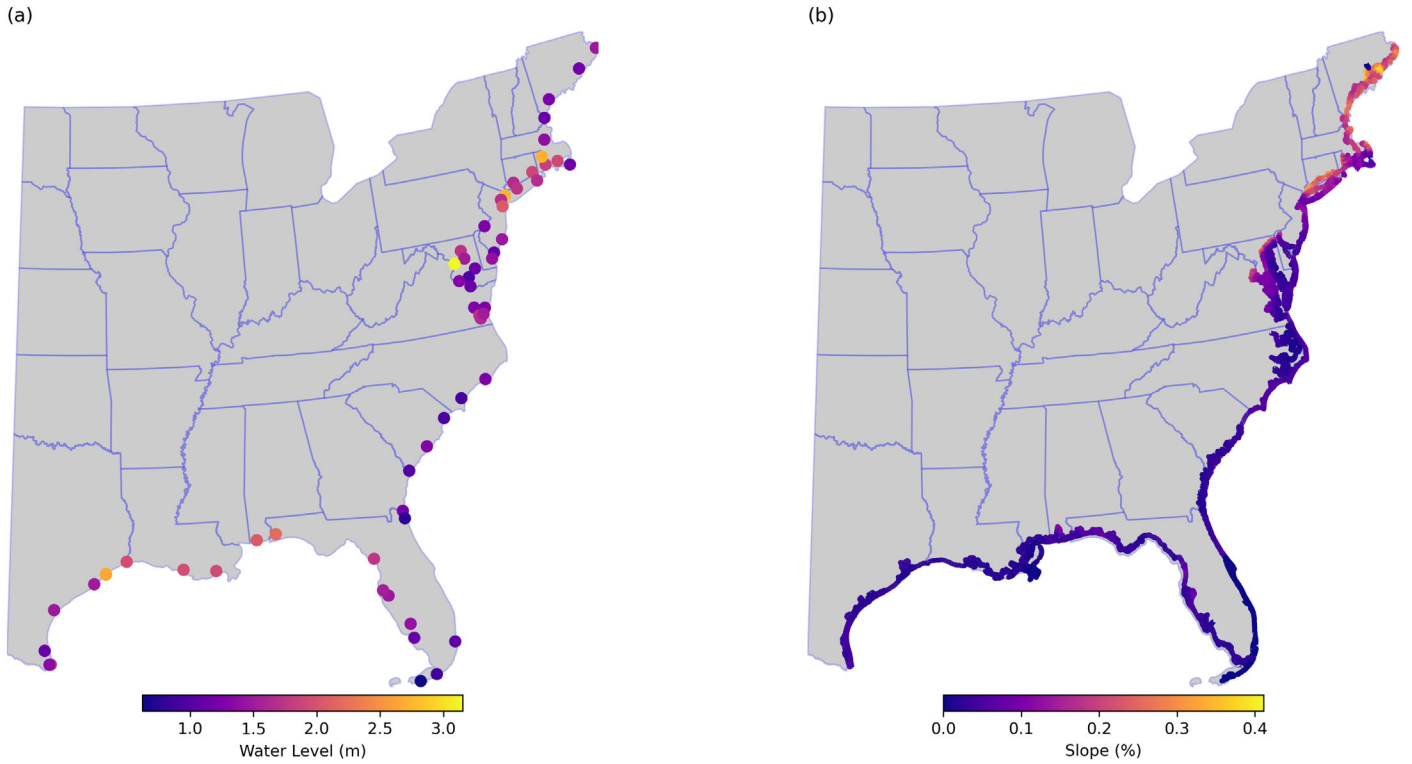
FIGURE 4. Map showing (a) extreme water levels with 1% exceedance probability above mean higher high water (MHHW) and (b) coastal slope.
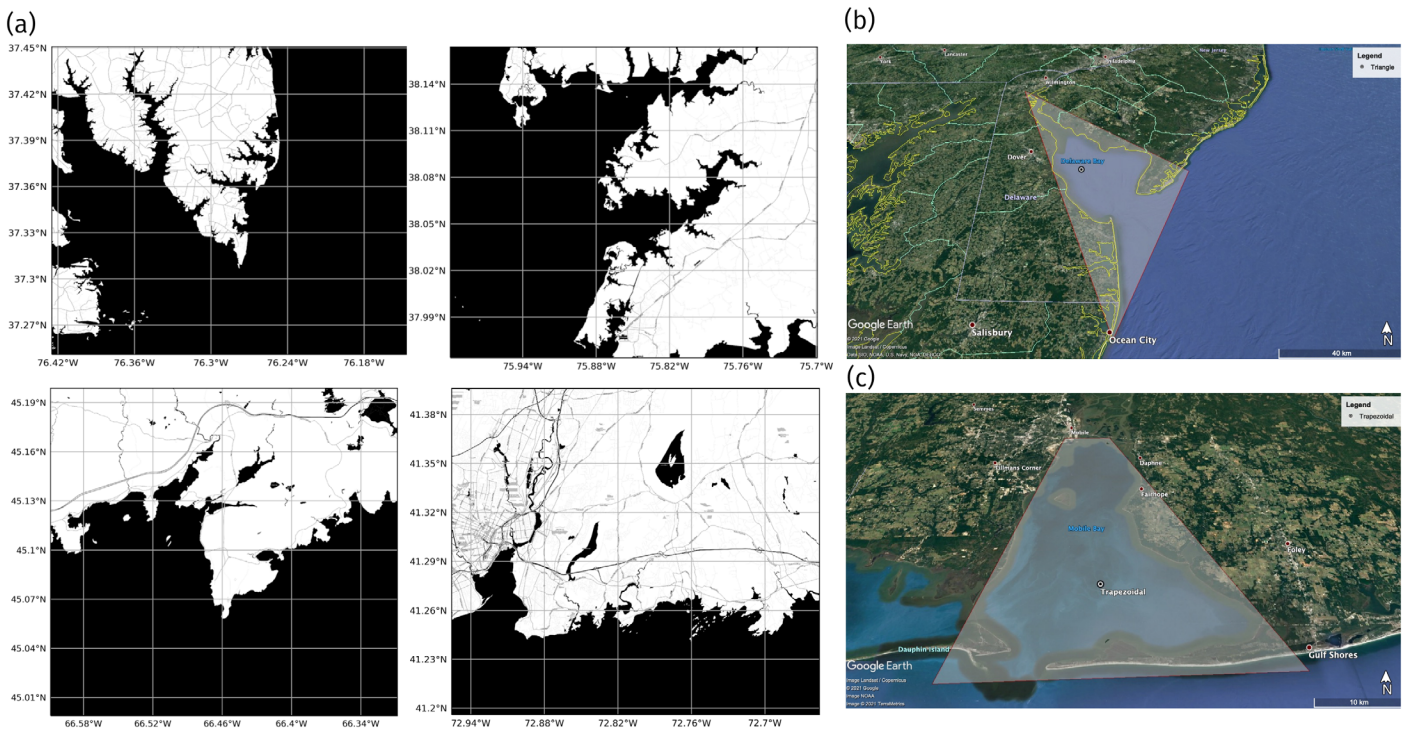

FIGURE 5. Examples of (a) satellite images that were retrieved for classifying CTZs along the United States (U.S.) East and Gulf coast, as well as manual labeling and shape delineation for (b) triangular and (c) trapezoidal estuaries.
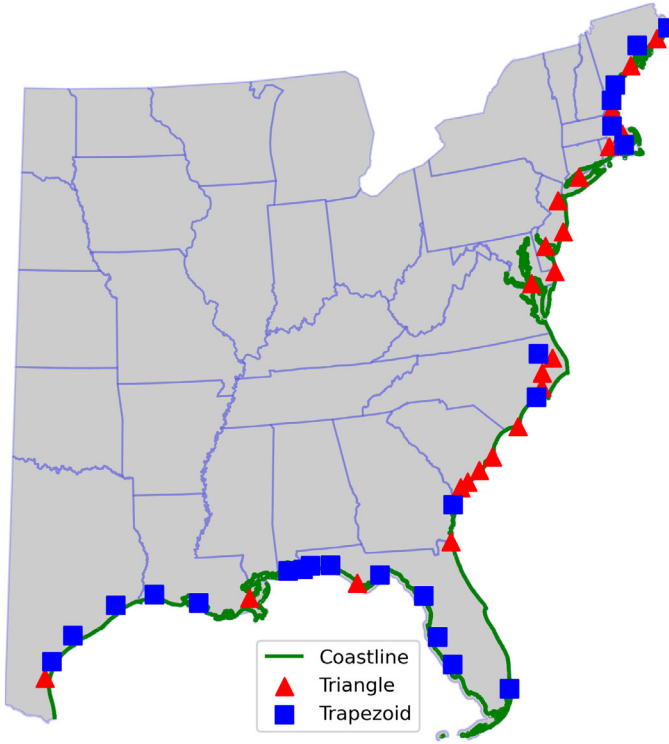
FIGURE 6. Map showing the spatial distribution of the selected 46 triangular- and trapezoidal-shaped river-estuary systems (RESs) in the study region.

The manual labeling of RESs in the region suggests that either there is no estuary (direct river–coast connection), or the estuaries are mainly triangular or trapezoidal shaped. For parameterizing these geometries, we further narrow down the obtained RES images to 46 cases where sizes of their geometric shapes are representative of the whole collection (Figure 6). We introduce three ratios to establish relationships among them, as follows:

$$R_{lb} = \frac{L_b}{W_b}, \qquad (3)$$

$$R_{bt} = \frac{W_b}{W_t}, \qquad (4)$$

$$R_{br} = \frac{W_b}{W_r}, \qquad (5)$$

where L_b is the estuary length, W_b is the downstream estuary width, W_t is the upstream estuary width (for trapezoidal estuaries), and W_r is the river width (Figure 7a). We should note that our parameterization and delineation strategies are specific to the region of our study and are not a general classification of

coastal areas. Thus, applying this framework to other regions will probably require modifications to the shapes and their parameters.

Based on a statistical analysis of the 46 RESs, the mean and median of R_{br} are 10.1 and 8.1 respectively, with higher values appearing above a latitude of 37°. Moreover, the median of R_{lb} is 2.2 and triangular shapes usually have higher values and are between latitudes 32° and 38° (Table 2).

Consequently, we categorize the CTZs into three classes, namely, without estuary (direct river–coast connection) (C1), triangular-shaped estuary (C2), and trapezoidal-shaped estuary (C3). Additionally, to account for other geometric elements with significant effects in hydrodynamic modeling of RESs, we introduce three categories within each class: a straight-line river (A), a sinuous river (B), and an estuary with island barriers (C) (Figure 7b).

Modeling Using Idealized Domains

Mesh and Physical Properties. We generate an idealized domain for each category and class (Figure 7b), each of which has two or three segments (ocean, estuary, and river) according to their respective classes.

We consider Category 1 models as the reference model when investigating multiple categories. We set the length of the ocean segment to 100 km (perpendicular to the coast) and its width to 50 km width (parallel to the coast) for ensuring that boundaries do not affect the region of interests (Figure 8a). Then, we generate the ocean mesh with approximately 17K nodes with varying grid resolution between 250 m and 1 km. Based on the mean of R_{br} values, we set the length of the river segment for the reference model (Category 1) to 1,000 km, and its width (W_r) to 1 km. The grid spacing of the river mesh is 250 m in the width direction and 1 km along the river (approximately 5K nodes). Considering the geometric shapes in our study, we adopt the downstream width of the estuary (W_b) as the independent parameter for scaling the idealized models. For all configurations with estuaries (Classes 2 and 3), we set W_b to 10 km, based on the sampling mean and median of the data (Table 2). Moreover, the estuary length (L_b) for the reference case is 20 km which is the median value of R_{lb}. The estuary mesh resolution varies between 250 m and 1 km, providing a smooth transition between the ocean and the river (approximately 2K nodes). Figure 8b depicts an example of such a mesh that we generated for the model C2A.

The bathymetry is variable parallel to the river direction and constant along the perpendicular to the river direction. Figure 8 shows the bottom elevation
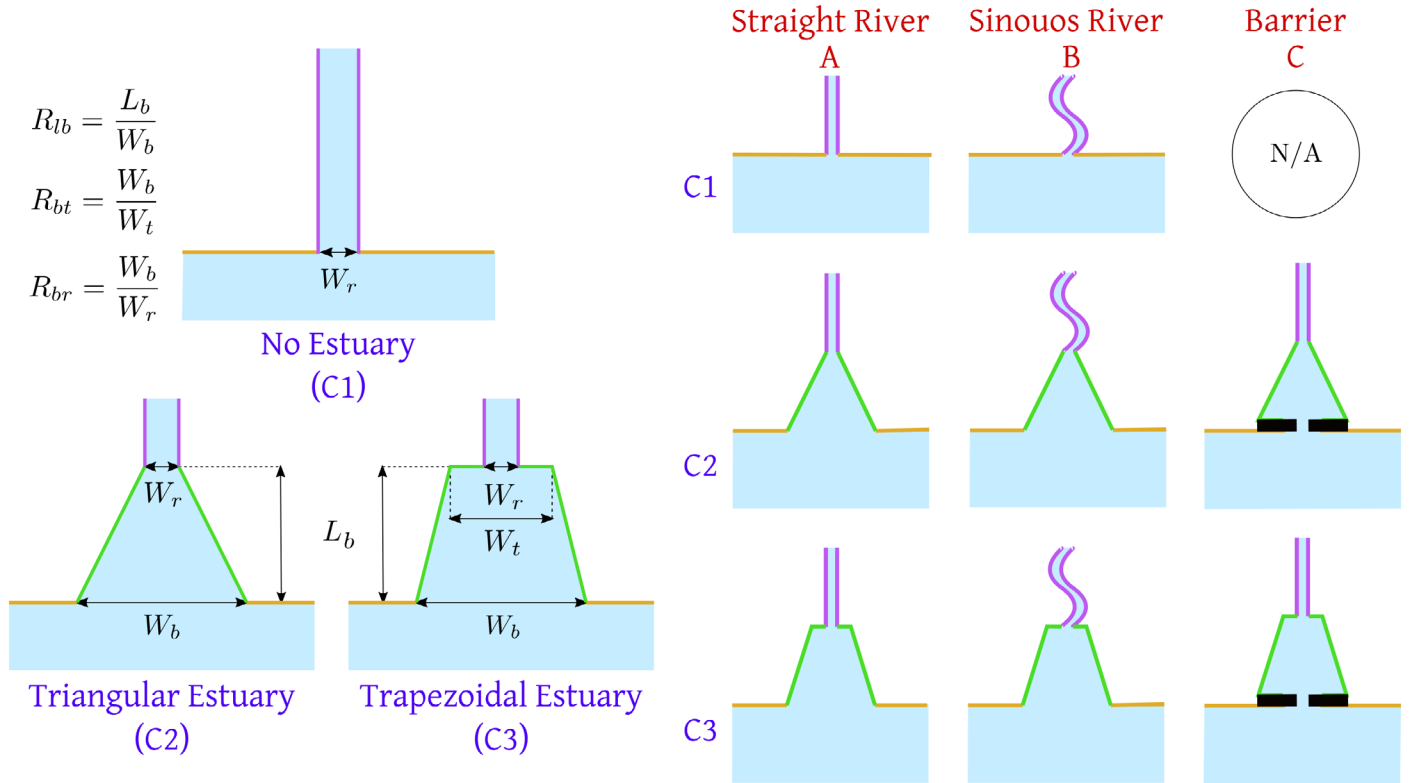
FIGURE 7. A depiction of geometry measurements and labels in the classification. Classes are C1 for without estuary, C2 for triangular-shaped estuary, and C3 for the trapezoidal-shaped estuary. Categories are A for the straight-line river, B for the sinuous river, and C for estuary with barriers.

TABLE 2. Summary statistics of the representative dimensions of the 46 satellite images of RESs.

Statistic	W_b, km	R_{bt}	R_{br}	R_{lb}
Mean	11.9	17.2	10.1	4.7
Standard deviation	11.3	23.2	14.	5.7
Minimum	0.4	0.23	0.75	0.67
Median	8.9	1.7	8.1	2.2
Maximum	49	79	90	25

of the domain. Based on the collected coastal slope data (Figure 4d), we use 0.055% for the bed slope of the ocean segment for all the models. At the river mouth, we choose a value for the depth larger than the maximum tidal amplitude to minimize the influence of the bottom in the tidal wave propagation and avoid the wave amplification as a result of bottom-wave interaction. Also in the river segment, we set the bottom elevation at the upstream boundary to −1 m, allowing the water to propagate upstream, and enabling the estimation of the TVP and delineation of the CTZ.

For Category B, we consider a river sinuosity of 1.45. The sinuosity is the ratio of channel length over valley length. For Category C, we set the opening of the barriers that enclose the mouth of the estuary to

2 km, equivalent to 20% of the estuary width. While Categories B and C were also implemented and studied, for brevity, in the Results section we only present the results of Category A (straight river) for the three classes.

We conduct the simulations using the hydrodynamic model, D-Flow Flexible Mesh (D-Flow FM) of the Delft3D Flexible Mesh Suite developed by Deltares (2019), with unstructured grids configured to perform 2D simulations. Although we use idealized domains to demonstrate this framework, the D-Flow FM solves the Navier–Stokes equations for an incompressible fluid, under the shallow water and the Boussinesq assumptions (Deltares 2019), which can represent complex nonlinear processes such as tidal propagation, backwater effect, and turbulence.

Boundary Conditions and Scenarios. We select a set of scenarios to perform the simulations and boundary conditions using ground-truth and remote sensing data. Based on the reference scenarios, we establish a procedure for setting up simulation by only changing one parameter per scenario, allowing the quantification of the contribution of the input parameters to the output results. We define these simulation scenarios based on uniform
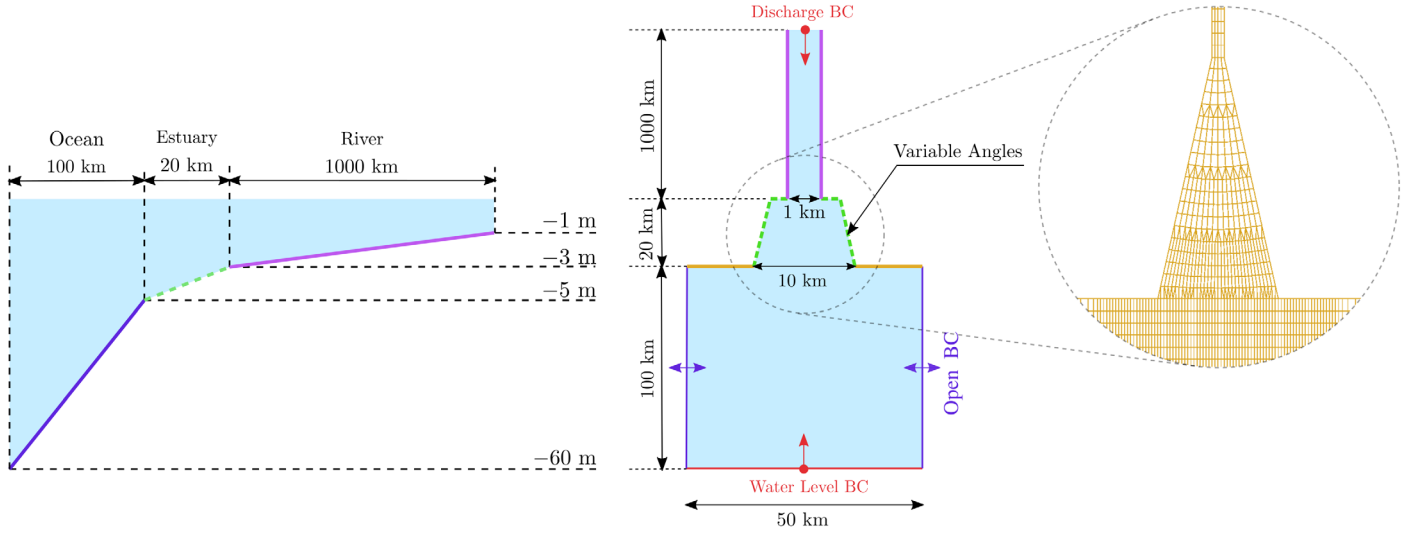
FIGURE 8. The reference model configuration. BC, boundary condition.

TABLE 3. Configurations of simulation scenarios. The water level at the ocean boundary (T) uses a water level time series based on NOAA's predicted tides (P) and the same predicted tides with a storm surge pulse superimposed (S).

Scenario	Roughness (R)	Discharge (D) [m³/s]	Ocean boundary (T)
Reference	0.025	0	P
R20	0.020	0	P
R30	0.030	0	P
S07	0.025	0	S = 0.769 m
S31	0.025	0	S = 3.154 m
D90	0.025	90	P
D570	0.025	570	P

Manning's roughness at the bed level (R), the upstream river discharge (D), and the water level at the ocean boundary (T). We use two types of water level time series at the ocean boundary — predicted tides (P) and storm surge that superimposes a surge pulse onto the predicted tides (S) (Table 3).

We select a location for obtaining water level data based on proximity to a station from the National Oceanic and Atmospheric Administration's (NOAA) National Water Level Observation Network (NWLON) with a considerable number of samples of higher tide amplitude during an extreme event. In this study, we opt for the NOAA station at Atlantic City, NJ (Lat = 39°21.4′N, Lon = −74°25.1′, ID = 8534720) where Hurricane Sandy made landfall (October 22–29, 2012). Subsequently, we use the water level predictions by NOAA's Operational Oceanographic Products and Services (CO-OPS) at this station during October 10–November 10, 2012 as the baseline water level boundary condition at the ocean boundary (Figure 9) for all scenarios. Following

the approach presented in Perrin et al. (2021) for storm surge analysis, we superimpose an isosceles triangular surge pulse on the baseline water level time series. However, instead of their parametrization approach, we consider the surge peak height (amplitude) as the only surge parameter and use a constant duration of two days for the rising and falling limbs of the pulse. Then, we produce two storm surge scenarios, S07 and S31, based on the minimum (0.769 m) and maximum (3.154 m) values of extreme water levels (above MHHW) that we obtained over the Gulf and U.S. East coast during 2000–2015 period.

For the reference scenario, we set the discharge at the upstream boundary to 0 m³/s. Then, we define two discharge scenarios (D) based on the mean of mean (90 m³/s) and mean of peak (570 m³/s) values that we obtain from the analysis of discharge data from USGS stations under the tidal influence (Figure 3). We use 30 days as the simulation duration for the scenarios (October 10–November 10, 2012) with a warm-up period of five days, that is the analyses of the results are based on 25 days (October 15–November 10, 2012).

Assessment of Water Surface Height and Velocity Field

Significance Test. In this study, we opt for using the MAE as a metric for measuring the total change between a scenario and the reference scenario. The significance test quantifies the relative significance of changes in a variable of interest between two competing predictions to a reference scenario (Jolliffe and
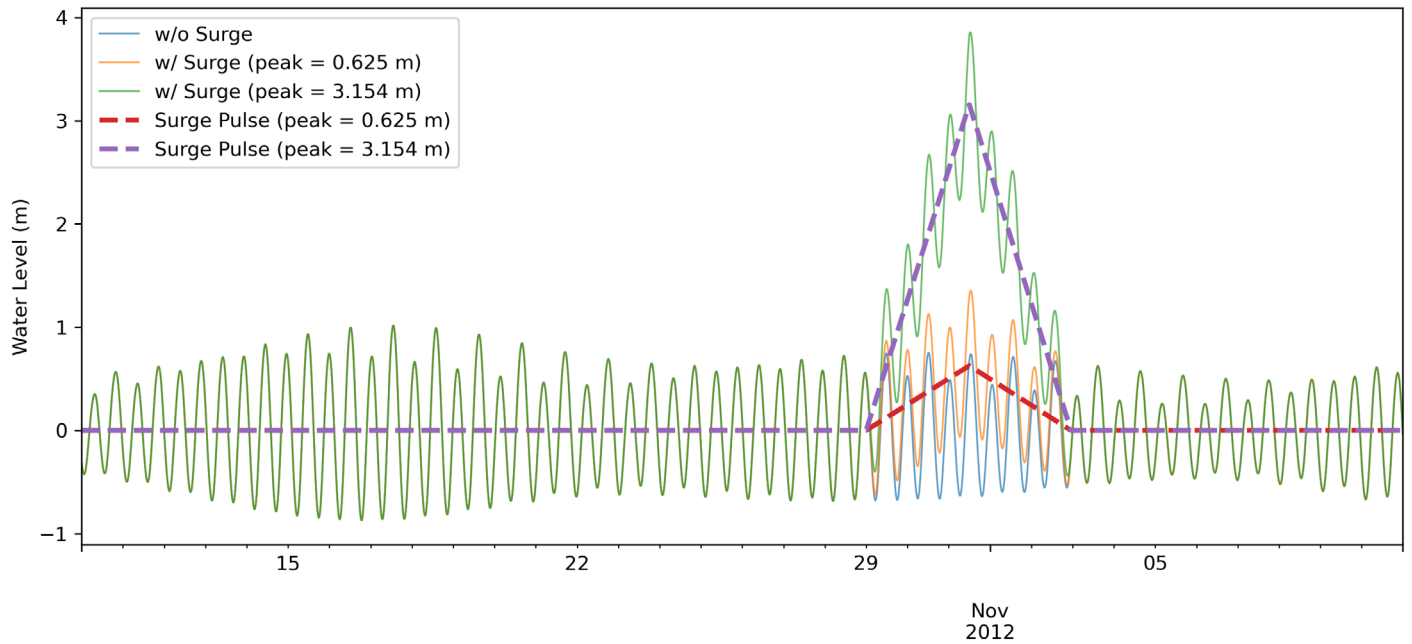
FIGURE 9. Water level time series for the ocean boundary condition based on NOAA's predicted tides and two surge pulses based on the 1% of exceedance probability above MHHW. We determine the peak values of 0.769 and 3.154 m based on extreme water levels (above MHHW) that we obtained over the Gulf and U.S. East coast during the 2000–2015 period.

Ebert 2017). We consider the water surface height and velocity field as the variables of interest and adopt 95% as the confidence level.

Tidal Vanishing Point. In the case study, we take into account three of the four tidal constituents' categories, namely semidiurnal, diurnal, and short period (overtides). As the simulation period in our study is one month, we do not include the long-period tidal constituents. For determining the dominant tidal constituent(s) in each category, we compare fluctuations of their amplitudes across the domain. Additionally, with trial-and-error, we determine the filtering window width of 2% of the centerline length and adopt 50% exceedance probability as the threshold to estimate TVPs for each scenario.

RESULTS AND DISCUSSION

In this section, we present the results obtained from the application of our proposed framework to the U.S. Gulf and East coast. While not attempting to provide a comprehensive analysis of all parameters contributing to TWL predictions, this section details the required steps for effective implementation of the framework and elucidates interpreting the outputs for gaining insights into the interplay of the parameters.

Significance Test

Figures 10 and 11 show the spatial distribution of the MAE Significance Test for water surface height and velocity field, respectively. The rows correspond to the parameters, that is, discharge (D), bed roughness (R), and storm surge (S), while columns are the classes, that is, without estuary (C1), triangular-shaped estuary (C2), and trapezoidal-shaped estuary (C3). For a specific parameter and class, the values in the color bar on the right indicate the relative significance of the changes in the corresponding scenarios.

Discharge. The significant difference in the discharge scenarios is shown in Figure 10a–10c, where greater differences are observed above approximately 300 km through the upland (y-axis) and are more pronounced in the higher discharge scenario (D570). In the lower river reach and estuary, there is no significant difference between both discharge scenarios. When there is no estuary (Figure 10a), there is a significant difference in water surface heights along the longer part of the river section in comparison to the other classes (Figure 10b and 10c). This difference suggests that the estuary area attenuates the tidal energy coming from the ocean. However, as we approach the mouth of the river, the discharge has a stronger influence on water level (Figure 10b and 10c) and velocity field (Figure 11b and 11c) in the
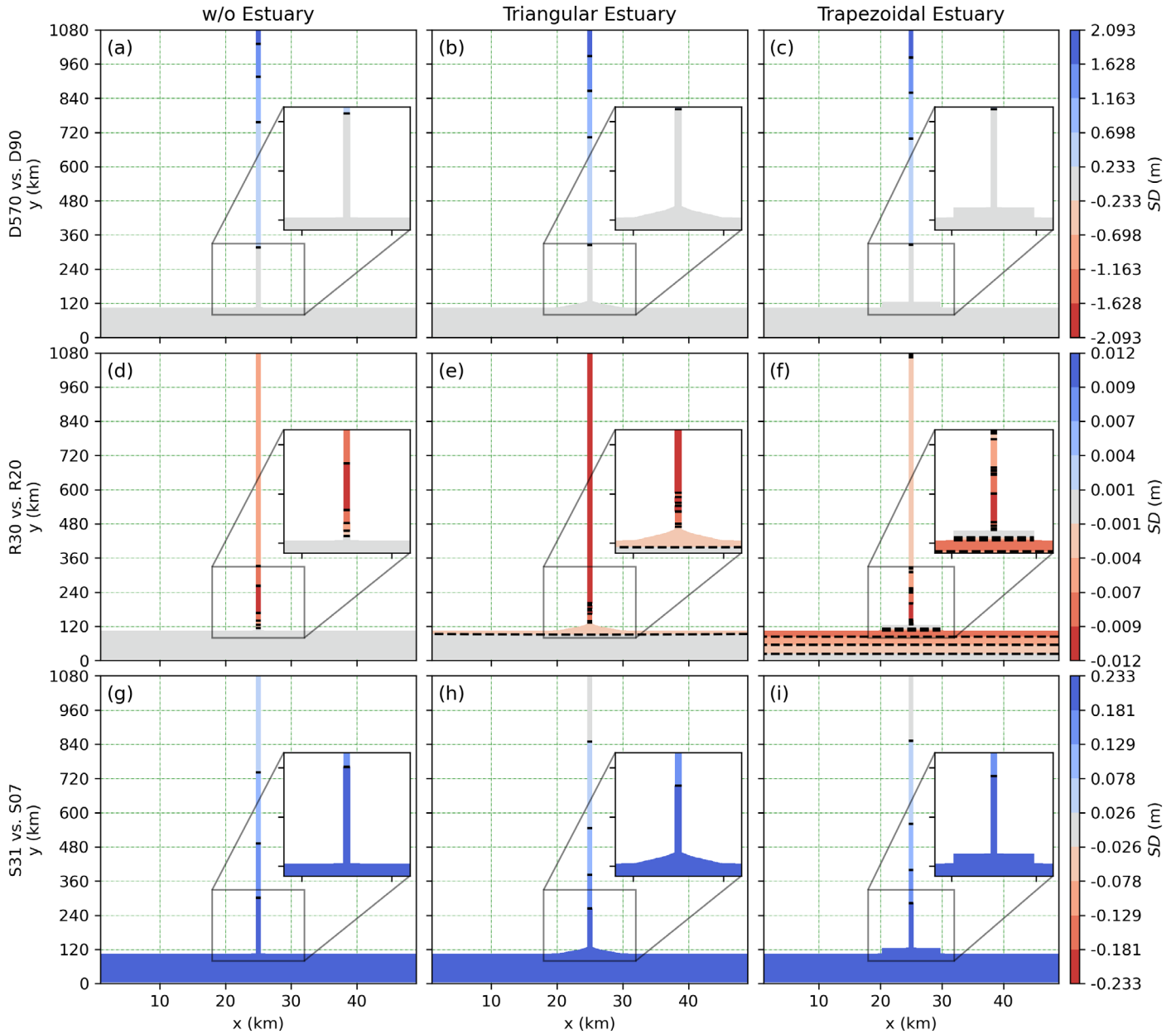
FIGURE 10. Mean absolute error (MAE) significance test results for the water surface heights. Each idealized domain class ((a), (d), and (g): without estuary, (b), (e), and (h): triangular estuary, and (c), (f), and (i): trapezoidal estuary) is presented in one column, while the scenario comparison is shown in each row (D570 vs. D90: discharge, R30 vs. R20: roughness, and S31 vs. S07: storm surge).

cases with an estuary. Additionally, we note the stronger influence of discharge in the river segment in Class 3 (Figures 10c and 11c), where the sharper edges of the trapezoidal-shaped estuary increase the dissipation of the tidal energy that enters the domain from the ocean boundary. Calero Quesada et al. (2019) reports a similar finding in their study of Guadiana estuary, in Spain. Harrison et al. (2021) also found that the impact of higher discharges is more relevant in upper and smaller estuaries while investigating two estuaries in the UK.

Roughness. In the bed roughness scenarios, since there is no river discharge in the upstream boundary, the tide from the ocean boundary is the only force in the domain. The reduction of Manning's roughness in scenario R20 results in a significant difference in comparison to the R30 scenario (Figures 10d–10f and 11d–11f) which corroborates the findings of Akbar et al. (2017) in their study on Hurricane Rita. Also, there is a greater difference in water level in Class 2 along the river.

Some studies (e.g., Savenije and Veling 2005; Van Rijn 2011) have shown that the balance between the
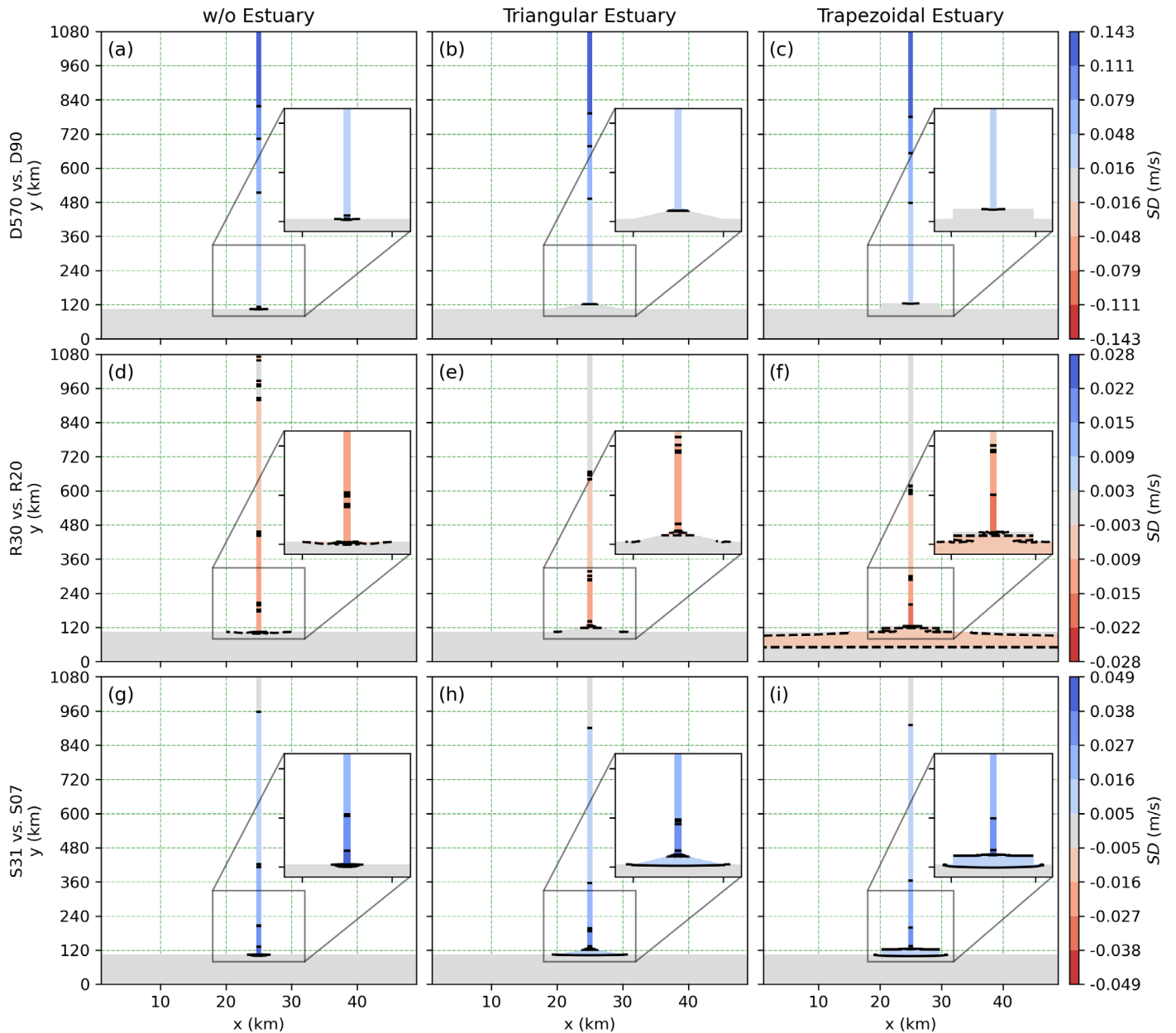
FIGURE 11. MAE significance test results for the velocity field. Each idealized domain class ((a), (d), and (g): without estuary, (b), (e), and (h): triangular estuary, and (c), (f), and (i): trapezoidal estuary) is presented in one column, while the scenario comparison is shown in each row (D570 vs. D90: discharge, R30 vs. R20: roughness, and S31 vs. S07: storm surge).

rate of convergence of the channel and the bed friction influences the magnitude of wave propagation dampening through a channel. This additional convergence effect near the mouth of the river due to the triangular shape of the C2 class appears to shift this balance, thereby creating more significant differences due to changes in bed roughness values.

The significance of differences in the velocity field is stronger and goes farther upstream of the river when there is no estuary (Figure 11d). These results suggest that the estuary promotes tidal energy

attenuation and reduces the impact of the bed roughness changes along the river. Moreover, due to the higher dissipation of energy in the trapezoidal estuary because of the sharp edges, the greatest changes in the velocity field occur near the estuary, but they are weaker through the upland (Figure 11f).

Storm Surge. In this scenario analysis, we notice significant differences both in water level (Figure 10g–10i) and velocity field (Figure 11g–11i) for the higher storm surge peak (S31) scenario. Moreover, in both
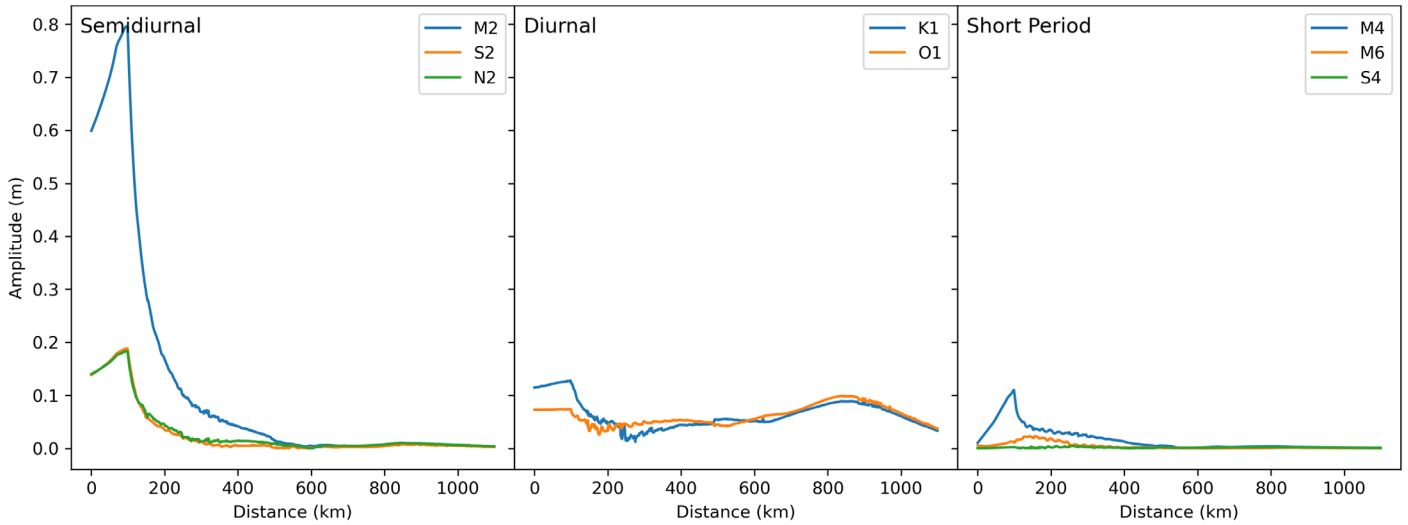
FIGURE 12. Example of the tidal constituent's dominance verification by categories for C1 D570 scenario (w/0 estuary and with river discharge set to 570 m³/s).
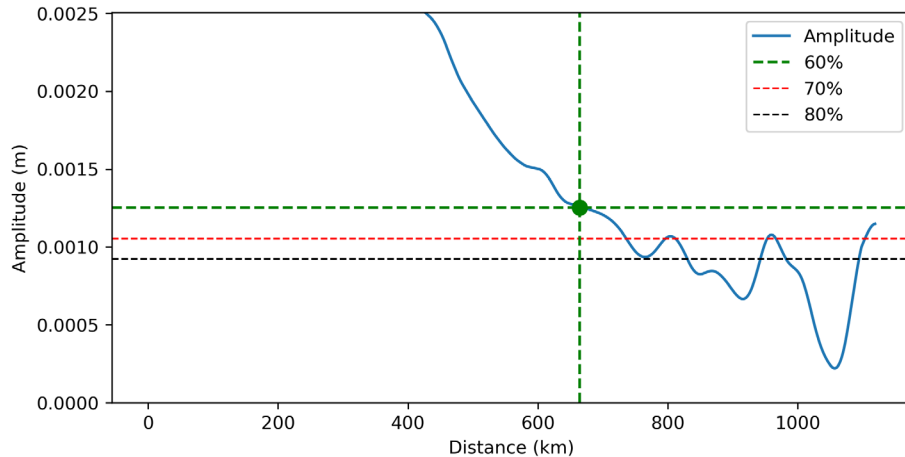

FIGURE 13. Example of the tidal vanishing point estimation for different exceedance probability levels.

cases, the storm surge leads to more prominent changes through the river in the without estuary case and these changes propagated farther through the upland (Figure 10g). Again, we see the attenuating role of the estuaries in these simulations, where a decrease in the significance values is observed when going upstream of the river (Figure 10h–10i). We notice no significant difference in the results for Classes 2 (Figures 10h and 11h) and 3 (Figures 10i and 11i).

Tidal Vanishing Point

In the analysis of the TVP, we apply the proposed framework considering three tidal constituents' categories: semidiurnal (e.g., M2, S2), diurnal (e.g., K1,

O1), and overtides or shallow-water tides (e.g., M4, M6) since the long period category is not applicable (simulation period is one month). First, we decompose the water level time series for each grid point along the centerline of the domain into its tidal constituents using the Python implementation of the UTide package (Codiga 2011). Then we identify the strongest tidal constituent of each category based on the obtained amplitudes. For example, Figure 12 shows a comparison of the constituents in each category for the C1 D570 scenario (without estuary and with river discharge of 570 m³/s). The results suggest that in the semidiurnal category, M2 is dominant; in the diurnal category, both O1 and K1 are dominant; and in the overtide category, M4 is the dominant constituent.
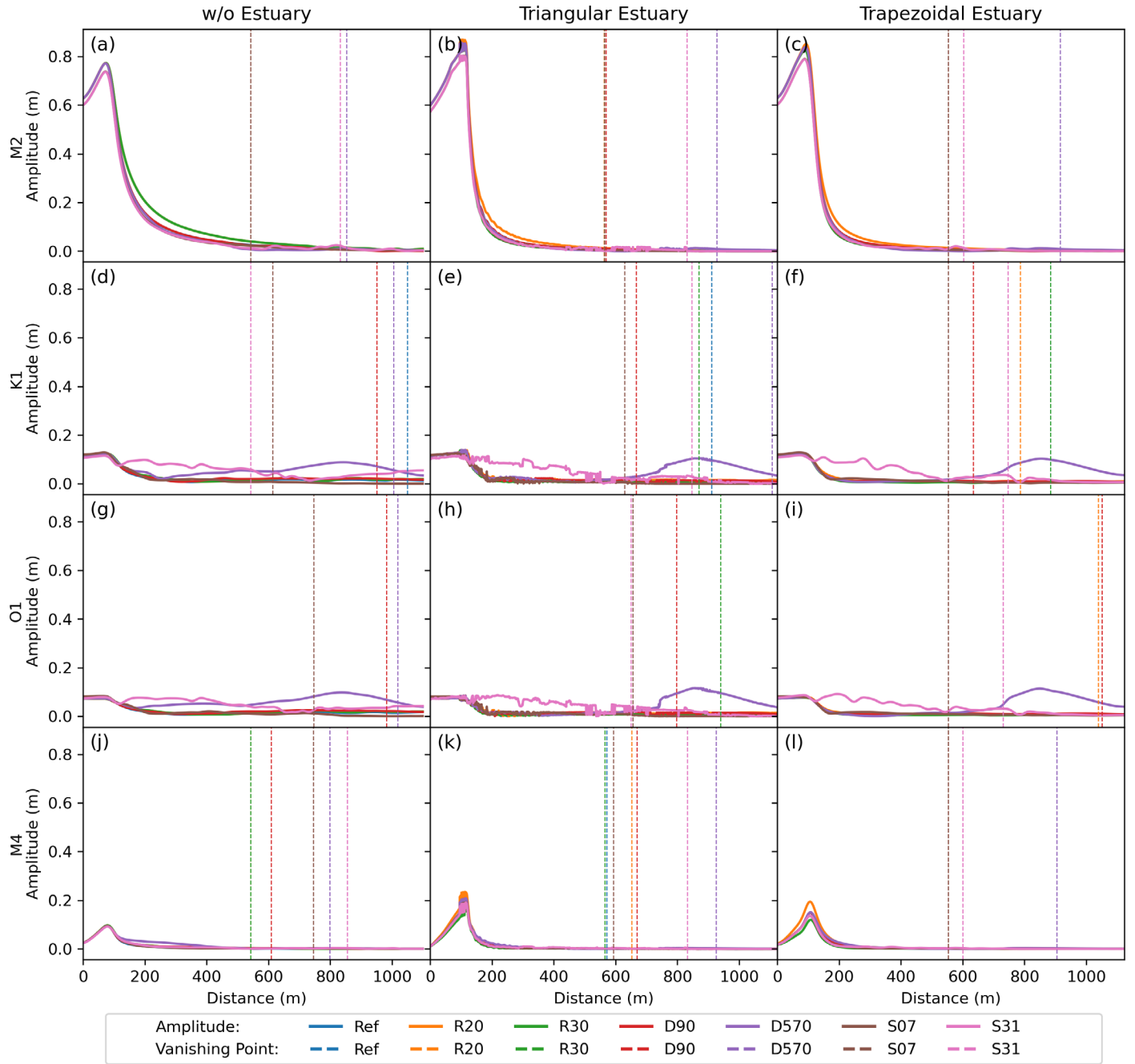
FIGURE 14. Tidal amplitude and vanishing point for the strongest tidal constituents in the scenarios.

Subsequently, we compute the rolling window average using a window width of 2% of the centerline length. We use a threshold value of the amplitude corresponding to the 50% exceedance probability for determining the TVPs. Figure 13 shows the effect of using different threshold values on the TVP estimation.

We carry out the significance test strategy based on the obtained values for the window width and the threshold. The results suggest that M2 is the dominant tidal constituent mainly in the ocean segment of the domain, while in the river segment K1 and O1 are stronger, especially when the river discharge is high. Moreover, M4 is the dominant overtide, with stronger influence near the estuary. Figure 14 shows the results of the tidal amplitude and TVP for the strongest tidal constituents (i.e., M2, K1, O1, and M4) in the selected categories, and Table 4 presents a summary of the obtained TVP locations.

TABLE 4. Locations of the tidal vanishing points relative to the ocean boundary in km.

Scenario	C1	C2	C3
Ref	OD[1]	1,123.5	OD
R20	OD	1,123.5	1,038.5
R30	OD	939.5	OD
S07	746.5	655.5	552.5
S31	OD	846.5	746.5
D570	1,018.5	1,123.5	OD
D90	981.5	797.5	1,050.5

[1]OD: outside the domain, that is the river length was not long enough to allow the amplitudes to fall below the threshold.

Semidiurnal Tidal Constituent. We notice a lower decay rate of the amplitude for the M2 tidal constituent for Class 1 (Figure 14a) in comparison to Classes 2 (Figure 14b) and 3 (Figure 14c), demonstrating the attenuation of the tidal propagation by the estuaries. In storm surge scenario S31, the tidal signal propagates farther upstream when compared with scenario S07 which has a lower surge peak. The TVP for the discharge scenario D570 does not show significant changes across the three classes.

Diurnal Tidal Constituents. The results for these constituents show higher amplitudes for scenarios S31 and D570 along the river reach (Figure 14d–14i). The K1 and O1 constituents are dominant, even stronger than semidiurnal constituents upstream of the river. Moreover, in the D570 case (Figure 14d–14i), the TVP occurs outside the domain, that is, the river is not long enough, so the two competing forces (tide from the ocean boundary and discharge from the river boundary) can reach an equilibrium.

Shallow-Water Tides. The results suggest that the TVPs are closer to the shore when increasing the bed roughness, that is, R30 vs. R20 (Figure 14j–14k). On the other hand, the results for the two surge scenarios show that the TVP in scenario S07 is closer to the ocean than for scenario S31 (Figure 14j–14l).

CONCLUSIONS

The objective of this study is to devise a top-down framework for investigating and conducting quantitative analysis of different processes and parameters that contribute to coastal hydrodynamics. We achieve this goal by parameterizing the physical processes that contribute to the complex coastal hydrodynamic behavior through analyses of ground-truth and remote sensing data in the region of interest and performing numerous simulations to study the significance of each process in isolation. The main findings are listed below:

1. We present a method to classify and parameterize CTZs that facilitates the correlation of the results found in the idealized models to real-world scenarios. We demonstrate this method by introducing one independent and three dependent variables for generating idealized CTZ domains based on the analysis of over 400 RESs along the U.S. East and Gulf coasts. Further investigations based on unexplored geometries and ratios would help to expand the applicability of the results to real-world scenarios.

2. The analysis of discharge demonstrates that although semidiurnal tidal constituents are dominant in most cases, as the discharge increases, diurnal tidal constituents become more dominant in the river segment. Therefore, the reach of tidal signals can extend farther through the upland as the discharge increases. Also, the analysis of bed roughness suggests that decreasing it promotes more significant changes in the results than increasing it by the same value. Moreover, the analysis of storm surge shows that the estuary promotes tidal energy attenuation and consequently decreases the reach of tidal signals through the upland.

3. We propose a novel method for delineating the reach of tidal signals through the upland called TVP based on the amplitude of dominant tidal constituents. This method can assist coastal and hydrological modelers with deciding on the handoff region between a computationally cheap inland model and a computationally expensive coastal model.

Although this study does not provide a comprehensive study of all parameters and complexities associated with the CTZs, the proposed framework is generic and extensible. It provides a systematic approach for determining the most significant processes and parameters influencing TWL predictions. The procedure could be applied to different coastal areas that would assist modelers during the processes of preparing, running, and analyzing coastal models.

DATA AVAILABILITY STATEMENT

The data that support the findings of this study are openly available in GitHub at https://github.com/cheginit/coastal_transition_zone.

AUTHOR CONTRIBUTIONS

Taher Chegini: Conceptualization; Data curation; Formal analysis; Investigation; Methodology; Software; Validation; Visualization; Writing – original draft; Writing – review & editing. **Gustavo de Almeida Coelho:** Conceptualization; Data curation; Formal analysis; Investigation; Methodology; Software; Validation; Visualization; Writing – original draft; Writing – review & editing. **John Ratcliff:** Conceptualization; Formal analysis; Methodology; Software; Validation; Writing – original draft; Writing – review & editing. **Celso Ferreira:** Conceptualization; Funding acquisition; Methodology; Project administration; Resources; Supervision; Writing – review & editing. **Kyle Mandli:** Conceptualization; Funding acquisition; Methodology; Project administration; Resources; Supervision; Writing – review & editing. **Patrick Burke:** Conceptualization; Funding acquisition; Project administration; Resources; Supervision; Writing – review & editing. **HongYi Li:** Funding acquisition; Writing – review & editing.

LITERATURE CITED

Akbar, M.K., S. Kanjanda, and A. Musinguzi. 2017. "Effect of Bottom Friction, Wind Drag Coefficient, and Meteorological Forcing in Hindcast of Hurricane Rita Storm Surge Using SWAN + ADCIRC Model." *Journal of Marine Science and Engineering* 5 (3): 38. https://doi.org/10.3390/jmse5030038.

Alebregtse, N.C., and H.E. de Swart. 2016. "Effect of River Discharge and Geometry on Tides and Net Water Transport in an Estuarine Network, an Idealized Model Applied to the Yangtze Estuary." *Continental Shelf Research* 123: 29–49. https://doi.org/10.1016/j.csr.2016.03.028.

Bakhtyar, R., K. Maitaria, P. Velissariou, B. Trimble, H. Mashriqui, S. Moghimi, A. Abdolali *et al.* 2020. "A New 1D/2D Coupled Modeling Approach for a Riverine-Estuarine System under Storm Events: Application to Delaware River Basin." *Journal of Geophysical Research: Oceans* 125 (9). https://doi.org/10.1029/2019JC015822.

Calero Quesada, M.C., J. García-Lafuente, E. Garel, J. Delgado Cabello, F. Martins, and J. Moreno-Navas. 2019. "Effects of Tidal and River Discharge Forcings on Tidal Propagation along the Guadiana Estuary." *Journal of Sea Research* 146: 1–13. https://doi.org/10.1016/j.seares.2019.01.006.

Camus, P., I.D. Haigh, A.A. Nasr, T. Wahl, S.E. Darby, and R.J. Nicholls. 2021. "Regional Analysis of Multivariate Compound Coastal Flooding Potential around Europe and Environs: Sensitivity Analysis and Spatial Patterns." *Natural Hazards and Earth System Sciences* 21 (7): 2021–40. https://doi.org/10.5194/nhess-21-2021-2021.

Chegini, T., H.-Y. Li, and L.R. Leung. 2021. "HyRiver: Hydroclimate Data Retriever." *Journal of Open Source Software* 6 (60): 3175. https://doi.org/10.21105/joss.03175.

Codiga, D.L. 2011. "Unified Tidal Analysis and Prediction Using the UTide Matlab Functions." Technical Report 2011-01. ftp://www.po.gso.uri.edu/pub/downloads/codiga/pubs/%0A2011Codiga-UTide-Report.pdf.

Couasnon, A., D. Eilander, S. Muis, T.I.E. Veldkamp, I.D. Haigh, T. Wahl, H.C. Winsemius, and P.J. Ward. 2020. "Measuring Compound Flood Potential from River Discharge and Storm Surge Extremes at the Global Scale." *Natural Hazards and Earth System Sciences* 20 (2): 489–504. https://doi.org/10.5194/NHESS-20-489-2020.

Deltares. 2019. "Delft3D Flexible Mesh Suite 1D/2D/3D Modelling Suite for Integral Water Solutions." User Manual D-Flow Flexible Mesh.

Du, J., J. Shen, Y.J. Zhang, F. Ye, Z. Liu, Z. Wang, Y.P. Wang, X. Yu, M. Sisson, and H.V. Wang. 2018. "Tidal Response to Sea-Level Rise in Different Types of Estuaries: The Importance of Length, Bathymetry, and Geometry." *Geophysical Research Letters* 45 (1): 227–35. https://doi.org/10.1002/2017GL075963.

Friedrichs, C.T., and D.G. Aubrey. 1994. "Tidal Propagation in Strongly Convergent Channels." *Journal of Geophysical Research* 99 (C2): 3321. https://doi.org/10.1029/93JC03219.

Garzon, J.L., and C.M. Ferreira. 2016. "Marine Science and Engineering Storm Surge Modeling in Large Estuaries: Sensitivity Analyses to Parameters and Physical Processes in the Chesapeake Bay." *Journal of Marine Science and Engineering* 4 (45). https://doi.org/10.3390/jmse4030045.

Ghanbari, M., M. Arabi, S.-C. Kao, J. Obeysekera, and W. Sweet. 2021. "Climate Change and Changes in Compound Coastal-Riverine Flooding Hazard Along the U.S. Coasts." *Earth's Future* 9 (5): e2021EF002055. https://doi.org/10.1029/2021EF002055.

Hammar-Klose, E.S., and E.R. Thieler. 2001. "Coastal Vulnerability to Sea-Level Rise: A Preliminary Database for the U.S. Atlantic, Pacific, and Gulf of Mexico Coasts." In *Data Series*. https://doi.org/10.3133/DS68.

Harrison, L.M., T.J. Coulthard, P.E. Robins, and M.J. Lewis. 2021. "Sensitivity of Estuaries to Compound Flooding." *Estuaries and Coasts* 1: 1–20. https://doi.org/10.1007/s12237-021-00996-1.

Hsiao, S.C., W.S. Chiang, J.H. Jang, H.L. Wu, W.S. Lu, W.B. Chen, and Y.T. Wu. 2021. "Flood Risk Influenced by the Compound Effect of Storm Surge and Rainfall under Climate Change for Low-Lying Coastal Areas." *Science of the Total Environment* 764: 144439. https://doi.org/10.1016/j.scitotenv.2020.144439.

Jay, D.A. 1991. "Green's Law Revisited: Tidal Long-Wave Propagation in Channels with Strong Topography." *Journal of Geophysical Research* 96 (C11): 20585. https://doi.org/10.1029/91JC01633.

Jena, B.K., K.M. Sivakholundu, and J. Rajkumar. 2018. "A Description of tidal Propagation in Hooghly Estuary Using Numerical and Analytical Solutions." *Ocean Engineering* 169: 38–48. https://doi.org/10.1016/j.oceaneng.2018.09.009.

Jolliffe, I., and B. Ebert. 2017. "How Do I Know Whether One Forecast System Performs Significantly Better Than Another?" https://www.cawcr.gov.au/projects/verification/CIdiff/FAQ-CIdiff.html.

Joyce, B.R., J. Gonzalez-Lopez, A.J. Van der Westhuysen, D. Yang, W.J. Pringle, J.J. Westerink, and A.T. Cox. 2019. "U.S. IOOS Coastal and Ocean Modeling Testbed: Hurricane-Induced Winds, Waves, and Surge for Deep Ocean, Reef-Fringed Islands in the Caribbean." *Journal of Geophysical Research: Oceans* 124 (4): 2876–907. https://doi.org/10.1029/2018JC014687.

Kerr, P.C., R.C. Martyr, A.S. Donahue, M.E. Hope, J.J. Westerink, R.A. Luettich, A.B. Kennedy, J.C. Dietrich, C. Dawson, and H.J. Westerink. 2013. "U.S. IOOS Coastal and Ocean Modeling Testbed: Evaluation of Tide, Wave, and Hurricane Surge Response Sensitivities to Mesh Resolution and Friction in the Gulf of Mexico." *Journal of Geophysical Research: Oceans* 118 (9): 4633–61. https://doi.org/10.1002/jgrc.20305.

Khalid, A., and C.M. Ferreira. 2020. "Advancing Real-Time Flood Prediction in Large Estuaries: iFLOOD a Fully Coupled Surge-Wave Automated Web-Based Guidance System." *Environmental Modelling and Software* 131: 104748. https://doi.org/10.1016/j.envsoft.2020.104748.

Lanzoni, S., and G. Seminara. 1998. "On Tide Propagation in Convergent Estuaries." *Journal of Geophysical Research: Oceans* 103 (C13): 30793–812. https://doi.org/10.1029/1998JC900015.

Maskell, J., K. Horsburgh, M. Lewis, and P. Bates. 2014. "Investigating River-Surge Interaction in Idealised Estuaries." *Journal of Coastal Research* 294 (2): 248–59. https://doi.org/10.2112/JCOASTRES-D-12-00221.1.

Moritz, H., K. White, and B. Gouldby. 2016. "An Updated USACE Approach to the Evaluation of Coastal Total Water Levels for Present and Future Flood Risk Analysis." *E3S Web of Conferences* 7: 01012. https://doi.org/10.1051/e3sconf/20160701012.

NOAA. 2016. "National Water Model: Improving NOAA's Water Prediction Services." http://water.NOAA.gov/documents/wrn-national-water-model.pdf.

NOAA. 2020. "NOAA Tides & Currents. Products. Datums. About Tidal Datums." https://tidesandcurrents.noaa.gov/datum_options.html.

Perrin, T.V.E., O. Roustant, J. Rohmer, O. Alata, J.P. Naulin, D. Idier, R. Pedreros, D. Moncoulon, and P. Tinard. 2021. "Functional Principal Component Analysis for Global Sensitivity Analysis of Model with Spatial Output." *Reliability Engineering and System Safety* 211: 107522. https://doi.org/10.1016/j.ress.2021.107522.

Savenije, H.H.G., and E.J.M. Veling. 2005. "Relation between Tidal Damping and Wave Celerity in Estuaries." *Journal of Geophysical Research C: Oceans* 110 (4): 1–10. https://doi.org/10.1029/2004JC002278.

Sohrt, V., S.S.V. Hein, E. Nehlsen, T. Strotmann, and P. Fröhle. 2021. "Model Based Assessment of the Reflection Behavior of Tidal Waves at Bathymetric Changes in Estuaries." *Water* 13 (4): 489. https://doi.org/10.3390/w13040489.

Talke, S.A., and D.A. Jay. 2020. "Changing Tides: The Role of Natural and Anthropogenic Factors." *Annual Review of Marine Science* 12 (1): 121–51. https://doi.org/10.1146/annurev-marine-010419-010727.

USGS. 2021. "USGS Site Type Codes (site_tp_cd)." https://maps.waterdata.usgs.gov/mapper/help/sitetype.html.

Valle-Levinson, A., M. Olabarrieta, and L. Heilman. 2020. "Compound Flooding in Houston-Galveston Bay during Hurricane Harvey." *Science of the Total Environment* 747: 141272. https://doi.org/10.1016/j.scitotenv.2020.141272.

Van Rijn, L.C. 2011. "Analytical and Numerical Analysis of Tides and Salinities in Estuaries; Part I: Tidal Wave Propagation in Convergent Estuaries." *Ocean Dynamics* 61 (11): 1719–41. https://doi.org/10.1007/s10236-011-0453-0.

Ward, N.D., J.P. Megonigal, B. Bond-Lamberty, V.L. Bailey, D. Butman, E.A. Canuel, H. Diefenderfer *et al*. 2020. "Representing the Function and Sensitivity of Coastal Interfaces in Earth System Models." *Nature Communications* 11 (1): https://doi.org/10.1038/s41467-020-16236-2.